Probing the in vivo changes in oxygen saturation with photoacoustic imaging as a non-invasive means of assessing treatment progression

Eno Hysi[1], Jonathan P. May[2], Lauren Writzfeld[1], Elijus Undyzs[3], Shyh-Dar Li[2], Michael C. Kolios[1,4]

[1]Department of Physics, Ryerson University, Toronto, Canada; [2]Faculty of Pharmaceutical Sciences, The University of British Columbia, Vancouver, Canada; [3]Drug Delivery and Formulation Group, Ontario Institute for Cancer Research, Toronto, Canada; [4]Li Ka Shing Knowledge Institute, Keenan Research Center, St. Michael's Hospital, Toronto, Canada
mkolios@ryerson.ca

ABSTRACT

In-vivo photoacoustic estimations of tumor oxygenation were used to assess the therapeutic efficacy of a thermosensitive liposome treatment in a pre-clinical mouse model. The treated group (n = 12) was administered doxorubicin-loaded, heat sensitive liposomes and exposed to mild hyperthermia (43°C) in order to deliver doxorubicin locally within the tumor micro-vessels. Control groups received systemic doxorubicin (n = 7) or saline (n = 12). The changes in tumor blood vessels after treatment were probed by analyzing the frequency content of the photoacoustic radiofrequency signals. Tumor oxygenation dropped by 15-20% during the first 30 minutes post-treatment when the tumors were exposed to encapsulated (Heat-Activated cyToxic – HaT-DOX) or free doxorubicin (DOX). The early (30 minutes to 5 hours) decrease in oxygen saturation strongly correlated to the reduction in tumor size assessed by caliper measurements. Control animals did not exhibit significant changes in tumor oxygenation at the early time points. The oxygenation at 7 days increased significantly for all groups. Measurements of the spectral slope from the normalized power spectra of the photoacoustic signals could also be used to differentiate between responder and non-responder mice. The results of this study suggest that photoacoustic imaging of tumors undergoing vascular-targeted cancer therapy can be used to assess treatment response early (hours) post-treatment through a combined analysis of oxygen saturation and photoacoustic radiofrequency spectroscopy.

Keywords: In vivo oxygen saturation, Photoacoustic imaging, Cancer treatment progression, Radiofrequency spectroscopy

1. INTRODUCTION

The vascular network of normal tissue branches hierarchically with a large degree of organization to ensure adequate delivery of nutrients to the cells of all organs. On the other hand, abnormal and dysfunctional blood vessels are a hallmark of solid tumors. Flaws in the vascular organization and function contribute to the malignant properties of cancer while preventing drugs from diffusing into the tumor [1]. Abnormally large pores in the tumor vessels cause leakage of fluid which increases the interstitial pressure exerted on the vessels. As a result, areas of low oxygenation are formed where conventional chemotherapy and radiation become ineffective. Several therapeutic approaches have been developed to either normalize the vessels in order to improve blood flow patterns [2] or destroy the vasculature starving the tumor of its nutrients [3]. Triggered drug release is an approach which focuses on delivering drugs localized within the tumor. The decreased systemic toxicity achieved through this localized delivery is a significant advantage that increases the efficacy of therapeutic payload. Thermosensitive liposomes (TSL) are an example of triggered drug delivery [4]. Encapsulating chemotherapeutic drugs inside heat-sensitive liposomes reduces the overall systemic toxicity, a common side effect of cancer drugs. Exposing the tumor to mild hyperthermia through an a non-invasive heating method causes the quick release of the drug at high local concentrations inside tumor vasculature enhancing its extravasation in the surrounding tumor cells [5], [6]. A commercially available TSL known as ThermoDox® (Celsion, Lawrenceville, NJ) is currently in Phase III clinical trials for hepatocellular carcinoma and Phase II trials for recurrent chest wall breast cancer [7]. In this study, a unique formulation of TSL was used to deliver doxorubicin (DOX).

Photons Plus Ultrasound: Imaging and Sensing 2015, edited by Alexander A. Oraevsky, Lihong V. Wang
Proc. of SPIE Vol. 9323, 93231Z · © 2015 SPIE · CCC code: 1605-7422/15/$18
doi: 10.1117/12.2080372

Compared to ThermoDox, this TSL (Heat-Activated cytoToxic – HaT-DOX) formulation releases its payload faster while retaining it better at physiological temperature.

Emerging evidence suggests that assessing cancer treatment efficacy early in the treatment could have a significant clinical impact [8]. Current practice is limited by the cost of operation of standard clinical imaging modalities such as magnetic resonance or positron emission tomography. Moreover, the need for external contrast agents makes these approaches impractical for routine monitoring of treatment response [9]. A modality capable of providing immediate, individualized feedback on treatment efficacy would afford oncologists the opportunity to adjust ineffective treatments sparing the patient physical and psychological side effects.

Photoacoustic (PA) imaging provides a unique means of assessing the efficacy of cancer treatments by probing the anatomy and physiology of tumor vasculature through the assessment of oxygen saturation (SO_2) [10]. Estimating tumor oxygenation after treatment can potentially provide information about functionality of tumor blood vessels as they undergo treatment. In addition, frequency analysis of the radiofrequency (RF) data can offer supplementary quantitative parameters to assess treatment response [11], [12]. In this study, acoustic-resolution PA imaging is employed to study the potential for assessing TSL therapeutic response hours after treatment by combining estimations of SO_2 with RF spectroscopy parameters.

2. METHODS

2.1 Treatment and imaging protocol

A total of 31 female, Balb/c mice (age 6-8 weeks, ~20 g, Jackson Labs (Bar Harbor, USA)) were inoculated with 2×10^5 EMT-6 murine mammary carcinoma cells (ATCC, Manassas, VA) in the left footpad. The tumors were grown for one week prior to treatment. Twelve mice were treated through an intravenous tail vein injection with HaT-DOX (Heat-Activated cytotoxic), a unique TSL designed to deliver doxorubicin (DOX) [5]. Seven other mice were treated with intravenous free DOX and the remaining twelve received vehicle control treatments of saline. After intravenous administration of drug or sham, the procedure consisted of immersing the tumor-bearing footpad in a 43°C water bath for 1 hour, sufficient to activate the triggered release of DOX from the TSL formulation in the treatment group. Each of the three groups underwent the mild hyperthermia exposure. Tumor growth was tracked by measuring the relative tumor dimensions using a caliper before treatment and for 30 days after treatment, or until endpoint was reached. Several animals in each group were sacrificed at 7 days for histological staining of the tumor. For each imaging and treatment session, the mice were anesthetized with isoflourane. All animal work was performed in accordance to protocols approved by the Animal Care Committee of the University Health Network (Toronto, Canada).

Animals were imaged using the VevoLAZR ultrasound (US) and photoacoustic (PA) imaging system (Fujifilm VisualSonics, Toronto, Canada) with a 40 MHz center frequency linear array probe coupled to optical fiber bundles. The laser (Nd:YAG) operated at 750 and 850 nm through an optical parametric oscillator (30 mJ/pulse, 6 ns pulse width, 20 Hz pulse repetition frequency). The animals were laid in prone position on a heated stage with the tumor-bearing leg extended and positioned below the probe before coupling with aqueous ultrasound gel. The US/PA probe was mounted to a 3D motor which enabled the scanning (6 mm range, 80 μm step size) of the entire tumor volume at each optical wavelength. For each 2D plane (14 mm lateral by 12 mm axial), co-registered US data was collected with the PA B-modes at each wavelength. All tumors were imaged pre-treatment (Pre) and 30 minutes (30m), 2 hours (2h), 5 hours (5h), 24 hours (24h) and 7 days (7d) post-treatment.

2.2 Oxygenation estimates

The RF data was reconstructed from the in-phase and quadrature components of the analytical US and PA signals measured by the imaging system. The PA data at both wavelengths were beamformed and corrected for the energy differences of each laser pulse. The US B-mode images of the tumor were used to manually segment the tumor region of interest (ROI). This ROI was applied to 21 PA B-mode images at 750 and 850 nm starting from the anatomical center of the tumor. The SO_2 value of each pixel was estimated using the two-wavelength approach [13]. A 2D moving average filter was used to produce a map of the oxygenation within the tumor. In order to quantify the SO_2 within the tumor, a histogram of SO_2 values within the tumor was computed for each of the 21. For each mouse, at every time point, the

average SO_2 histogram was computed from all 21 histograms. A combined average histogram was then computed for all animals within each treatment group.

2.3 PA RF spectroscopy

The same tumor segmentations that were used to compute the SO_2 histograms were applied to perform RF spectroscopy analysis. Within each 2D tumor ROI, the power spectrum was computed by performing the windowed Fourier Transform of every RF line that made up the tumor (80-100, depending on tumor size). The same ROI was applied to the PA image from a gelatin-based phantom consisting of 10 black, carbon beads per resolution volume of the transducer (diameter 2-12 μm, Sigma-Aldrich Co., St. Louis, MO). This homogenous phantom allowed for the normalization of the PA signals. The power spectra from the tumor ROI were subtracted from the depth-matched power spectra of the phantom ROI. This procedure was applied to 21 tumor ROIs per mouse for every time point for both wavelengths of illumination. The resulting normalized power spectra were fitted to a straight line in the -6 dB transducer bandwidth (25-40 MHz). The spectral slope was extracted for each frame and the frames were averaged to get an estimate at every time point. The normalized power spectra for a HaT-DOX responder and non-responder were chosen for analysis based on the treatment response as assessed by the tumor growth measurements performed using a caliper. The spectral slope (SS) was computed for all 21 frames at each Pre, 30m and 7d for both responding and non-responding mice.

3. RESULTS AND DISCUSSION

3.1 Oxygen saturation as a function of treatment

Figure 1 shows the average SO_2 histograms of the animals treated with (a) HaT-DOX, (b) DOX and (c) saline for all imaging time points. Compared to the Pre time point, the HaT-DOX and DOX histograms show a significant shift to the left at 30m suggesting that the oxygenation of treated tumors dropped. This 15-20% drop in SO_2 persisted up until 5h post-treatment. 24h after treatment, the oxygenation began to recover for both HaT-DOX and DOX. The quick and localized release of DOX through the liposome delivery vehicle seems to be correlated to the significant changes in tumor oxygenation as early as 30m post treatment. It is hypothesized that the accumulation of DOX in the endothelial cells potentially leads to microvascular cell death resulting in disruption in tumor blood supply and the early decrease in tumor oxygenation [14]. The systemic injection of DOX under mild hyperthermia has also been reported to increase the extravasation of the drug due to enhanced vessel permeability leading to enhanced antitumor effects. Injecting free DOX does not reduce the systemic exposure to the drug thus generating a similar level of overall toxicity compared to non-hyperthermic treatments [7].

By contrast, the saline-treated animals did not exhibit a significant change in their oxygenation post-treatment. On average, the histograms of this group appeared to exhibit bi-modal distributions, likely due to intertumoral heterogeneity and variability within the untreated tumor growth. At the 7d time point, the oxygenation of all treatment groups increased by ~20% from the pre-treatment levels. The histogram for the saline group was no longer bimodal suggesting that by 7d, the vascular functionality of the untreated tumors became more uniform across the control animals. It is worth noting that, on average, the changes in tumor size as assessed by caliper measurements did not became significant between the treatment groups and control until 14 days post treatment. However, the early (hour time scale) changes in the oxygenation of treated tumors were apparent between the treated and controlled groups. This suggests that PA estimates of tumor oxygenation can potentially serve as an early marker of treatment efficacy.

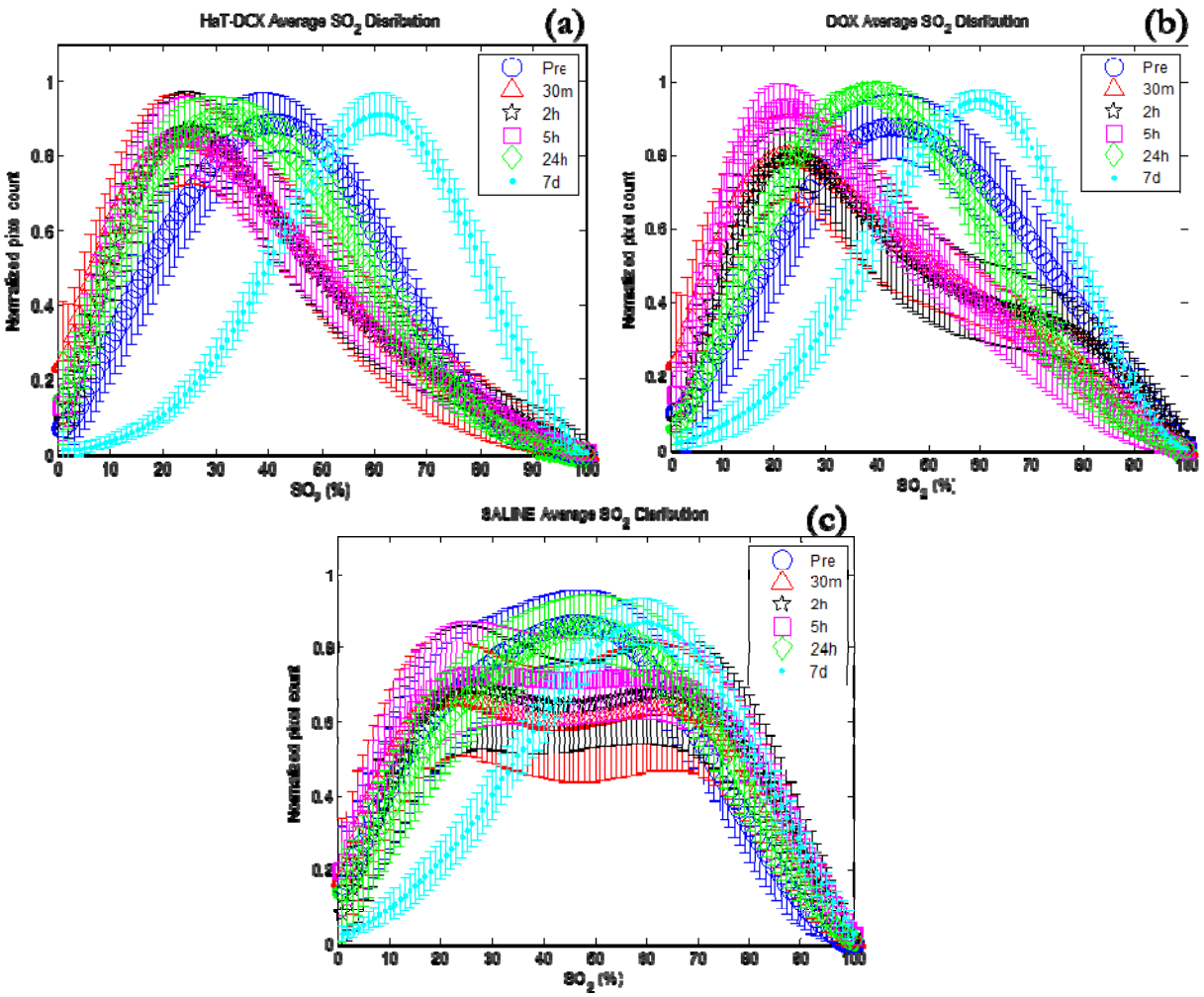

Figure 1: Average distributions of SO_2 for (a) HaT-DOX (n = 12), (b) DOX (n = 7) and (c) Saline (n = 12) as a function of time after treatment. Error bars represent the standard deviations of 21 oxygen saturation histograms for all mice in each treatment group.

3.2 HaT-DOX responder vs. non-responder

The tumor size was measured using a caliper in order to assess effect of treatment on the overall tumor growth. Figure 2(a) shows the normalized tumor sizes for 2 animals that received the HaT-DOX treatment on the same day. Here, 100% represents the tumor size estimate on the day of treatment. One of these animals (labelled responder) was followed to 7d at which point it was sacrificed for histology. It is apparent from this graph that this tumor responded to the HaT-DOX treatment since its size decreased post-treatment. The other mouse (labelled non-responder) exhibited a rather significant increase post-treatment until it was sacrificed (i.e. it grew to 300% of the tumor size on the day of treatment).

The SO_2 histograms for the HaT-DOX responder and non-responder are shown in figures 2(b) and 2(c), respectively. The histograms are only shown for the Pre, 30m and 7d time points in order to visualize the early and late changes in oxygenation. As seen in figure 2(b), the responder exhibited a significant drop (15%) in oxygenation at 30m post-treatment. In contrast, the non-responder oxygenation did not change significantly at the same time point (figure 2(c)). By 7d post-treatment, the responder oxygenation histogram had a mode of ~70% compared to a mode of ~50% for the non-responder. The significant changes in SO_2 between responding and non-responding mice are quite apparent using the histogram representation. The early drop in oxygenation for the responding mouse correlates well with the changes in the overall tumor size as seen in figure 2(a). On the other hand, the non-responder histograms provide a dynamic picture of the oxygenation of a tumor that did not respond to treatment. The strong correlation between tumor size (long term

measurement) and the physiological estimates of SO_2 (short term measurement) suggests that the therapeutic response can be assessed very early in the treatment process eliminating the need to wait for several days/weeks to establish treatment efficacy.

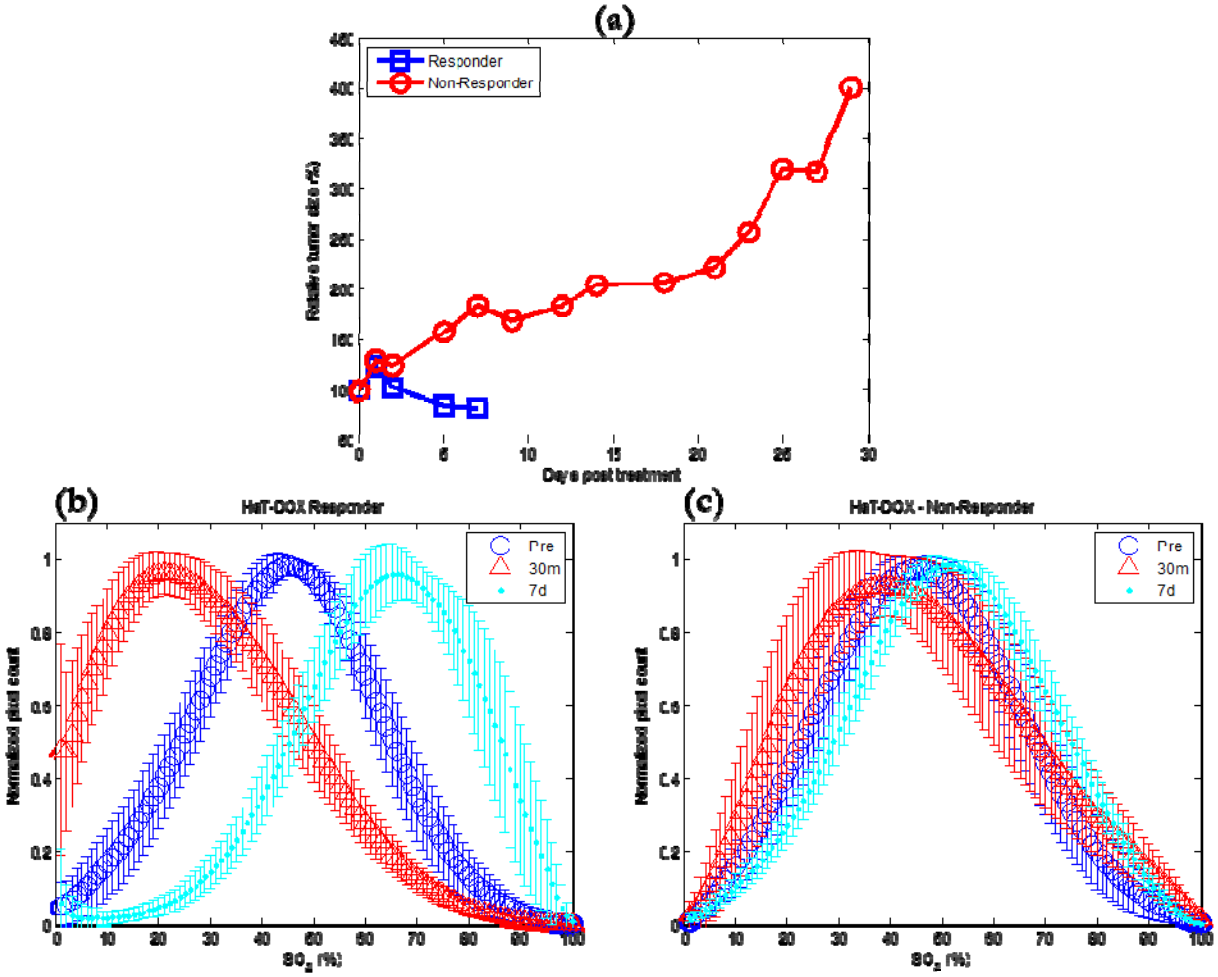

Figure 2: (a) Relative tumor size measurements for a HaT-DOX responder and a non-responder as a function of time post-treatment. (b) HaT-DOX responder and (c) HaT-DOX non-responder average oxygenation histograms for 3 time points of interest. The error bars represent the standard deviation of 21 histograms per mouse.

3.3 Normalized PA power spectra and quantitative spectral parameters

Figure 3 shows the normalized power spectra for the (a) HaT-DOX responder and (b) HaT-DOX non-responder at 750nm, 850 nm and 3 time points of interest. The amplitude of the power spectra at 750 and 850 nm is reflective of the changes in oxygenation that occur as a function of treatment time since it is proportional to the strength in the PA signal amplitude. On the other hand, the change in the spectral slope (SS) of the normalized spectra, shown in figure 4, can be indicative of the structural changes that occur in the vasculature of the tumors as a function of treatment. The variation in the amplitude of the power spectra within the responding mouse (figure 3(a)) decreases as early as 30m post treatment at 750 nm. This decrease in intratumoral heterogeneity is also reflected in the SS variance which decreases for the responding mouse at 30m as shown in figure 4. The SS decreases at 30m by 46% and by 111% at 7d at 750 nm. In contrast, the non-responding mouse does not exhibit a significant change in SS at 750 nm until the 7d time point when it decreases by 66%. At 850 nm, the SS of both mice decreases at 30m. However, the responding mouse exhibits a 5 fold decrease in SS while the non-responder only decreases by 2 fold. At 7d, the SS of the responding mouse is 35% lower than the non-responding mouse.

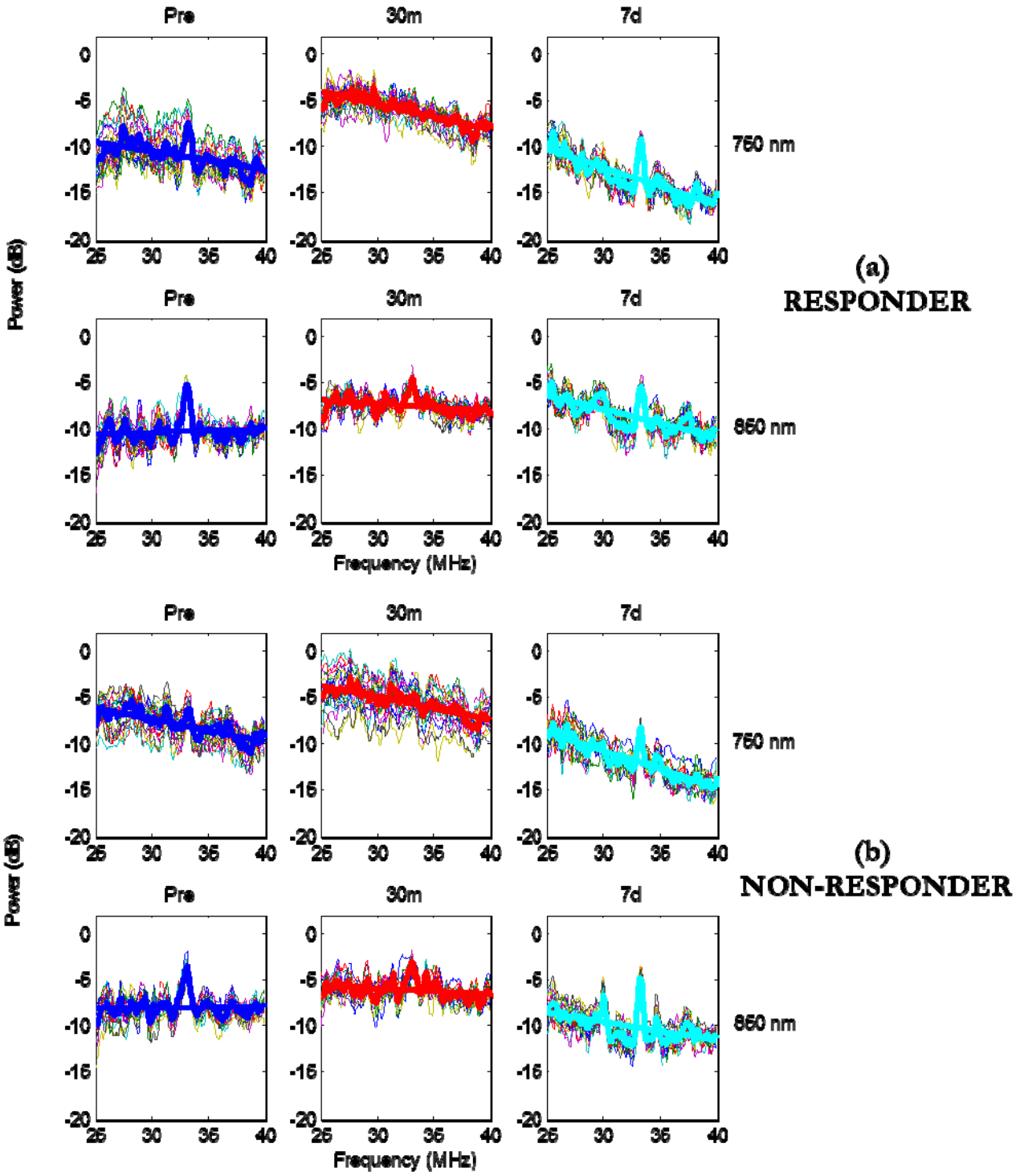

Figure 3: PA RF power spectra for the HaT-DOX (a) responder and (b) non-responder at Pre, 30m and 7d post-treatment. The top row contains power spectra from the 750 nm measurements and the bottom row contains power spectra from the 850 nm measurements. Each plot contains the power spectra of 21 imaging planes per time point along with the corresponding average power spectra (thick line).

The differences in the SS that are observed between responding and non-responding mice suggest that analysis of the frequency content of PA RF signals can provide information about the structure of tumor vessels, the dominant source of PA signals. Previous studies have shown that decreases in PA spectral parameters are correlated to changes in the size and concentration of the PA absorbers [11], [15]. In the context of therapeutic monitoring, these parameters could be used to quantify the structural changes that tumor blood vessels undergo during treatment by measuring the PA signals from the red blood cells. For a treatment such as HaT-DOX, it is hypothesized that the destruction of tumor blood vessels from the DOX-induced endothelial cell death could result in hemorrhaging within the tumor. Hemorrhaging could cause the red blood cells to pool and aggregate within the tumor interstitial spaces. These blood cell aggregates, creating an absorbing structure of increased size, will affect the photoacoustic signals – both in terms of PA signal strength, but also spectral slope [11]. The spectral analysis has the potential to provide a means of assessing the degree of hemorrhaging based on changes in parameters such as the spectral slope. However, it is not known how long the red blood cells will retain their structural integrity after a treatment-induced vascular collapse.

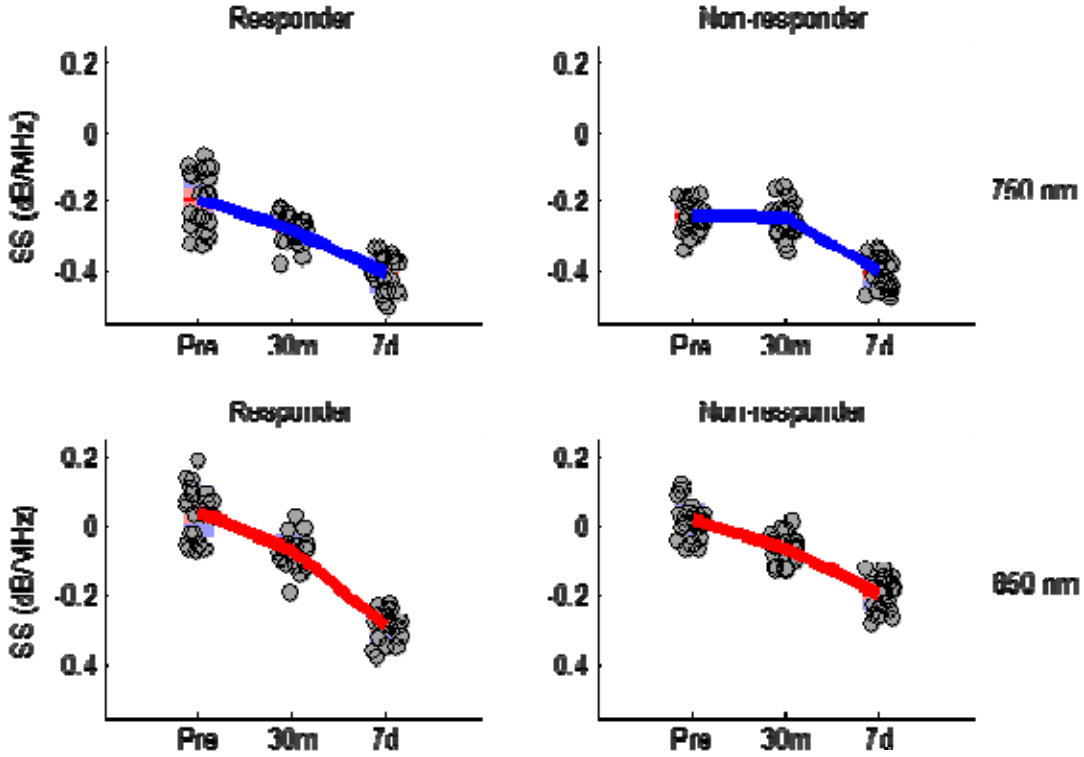

Figure 4: PA spectral slope (SS) of the normalized power spectra of the HaT-DOX responder and non-responder for the deoxygenated/750 nm (top row) and oxygenated/850 nm (bottom row) wavelengths. Each circle represents the mean SS at a given frame. The blue and red bars overlaid underneath each circle represent one standard deviation and one standard error of the mean (red horizontal line), respectively.

4. CONCLUSIONS

This paper investigated the potential of PA imaging for assessing the in-vivo treatment response of a unique TSL treatment. Combining PA estimates of tumor oxygenation with PA RF spectroscopy parameters provided a robust means of differentiating the response to HaT-DOX treatments. Changes in oxygenation, as early as 30m after administration of treatment, correlated well with the overall therapeutic response assessed by caliper measurements. Histograms of SO_2 distribution within the tumor provided a unique means of understanding the dynamics of oxygen delivery as a function of treatment progression.

5. ACKNOWLEDGMENTS

The authors would like to acknowledge the STTARR facility in Toronto for allowing use of their resources. This research was undertaken, in part, through the generous funding of the Canadian Institute of Health Research Proof of Principle Phase I grant awarded to S.D. Li, The Terry Fox New Frontiers Program Project Grant in Ultrasound and MRI for Cancer Therapy (project #1034) and the Canada Research Chairs Program awarded to M. C. Kolios. The technical support from Deborah Scollard (UHN) and Fujifilm VisualSonics is gratefully acknowledged.

REFERENCES

[1] P. Carmeliet and R. K. Jain, "Angiogenesis in cancer and other diseases," *Nature*, vol. 407, no. 6801, pp. 249–257, Sep. 2000.
[2] V. P. Chauhan, T. Stylianopoulos, J. D. Martin, Z. Popović, O. Chen, W. S. Kamoun, M. G. Bawendi, D. Fukumura, and R. K. Jain, "Normalization of tumour blood vessels improves the delivery of nanomedicines in a size-dependent manner," *Nat. Nanotechnol.*, vol. 7, no. 6, pp. 383–388, Apr. 2012.
[3] J. Folkman, "Fundamental concepts of the angiogenic process," *Curr. Mol. Med.*, vol. 3, no. 7, pp. 643–651, 2003.
[4] Q. Chen, S. Tong, M. W. Dewhirst, and F. Yuan, "Targeting tumor microvessels using doxorubicin encapsulated in a novel thermosensitive liposome," *Mol. Cancer Ther.*, vol. 3, no. 10, pp. 1311–1317, 2004.
[5] T. Tagami, M. J. Ernsting, and S.-D. Li, "Efficient tumor regression by a single and low dose treatment with a novel and enhanced formulation of thermosensitive liposomal doxorubicin," *J. Controlled Release*, vol. 152, no. 2, pp. 303–309, Jun. 2011.
[6] T. Tagami, J. P. May, M. J. Ernsting, and S.-D. Li, "A thermosensitive liposome prepared with a Cu2+ gradient demonstrates improved pharmacokinetics, drug delivery and antitumor efficacy," *J. Controlled Release*, vol. 161, no. 1, pp. 142–149, Jul. 2012.
[7] J. P. May and S.-D. Li, "Hyperthermia-induced drug targeting," *Expert Opin. Drug Deliv.*, vol. 10, no. 4, pp. 511–527, Apr. 2013.
[8] R. S. Punglia, M. Morrow, E. P. Winer, and J. R. Harris, "Local Therapy and Survival in Breast Cancer," *N. Engl. J. Med.*, vol. 356, no. 23, pp. 2399–2405, Jun. 2007.
[9] E. Yeh, P. Slanetz, D. B. Kopans, E. Rafferty, D. Georgian-Smith, L. Moy, E. Halpern, R. Moore, I. Kuter, and A. Taghian, "Prospective comparison of mammography, sonography, and MRI in patients undergoing neoadjuvant chemotherapy for palpable breast cancer," *AJR Am. J. Roentgenol.*, vol. 184, no. 3, pp. 868–877, Mar. 2005.
[10] L. V. Wang and S. Hu, "Photoacoustic Tomography: In Vivo Imaging from Organelles to Organs," *Science*, vol. 335, no. 6075, pp. 1458–1462, Mar. 2012.
[11] E. Hysi, R. K. Saha, and M. C. Kolios, "Photoacoustic ultrasound spectroscopy for assessing red blood cell aggregation and oxygenation," *J. Biomed. Opt.*, vol. 17, no. 12, pp. 125006–125006, 2012.
[12] M. P. Patterson, C. B. Riley, M. C. Kolios, and W. M. Whelan, "Optoacoustic characterization of prostate cancer in an in vivo transgenic murine model," *J. Biomed. Opt.*, vol. 19, no. 5, pp. 056008–056008, 2014.
[13] X. Wang, G. Ku, M. A. Wegiel, D. J. Bornhop, G. Stoica, and L. V. Wang, "Noninvasive photoacoustic angiography of animal brains in vivo with near-infrared light and an optical contrast agent," *Opt. Lett.*, vol. 29, no. 7, pp. 730–732, 2004.
[14] Q. Chen, A. Krol, A. Wright, D. Needham, M. W. Dewhirst, and F. Yuan, "Tumor microvascular permeability is a key determinant for antivascular effects of doxorubicin encapsulated in a temperature sensitive liposome," *Int. J. Hyperthermia*, vol. 24, no. 6, pp. 475–482, Jan. 2008.
[15] E. Hysi, R. K. Saha, and M. C. Kolios, "On the use of photoacoustics to detect red blood cell aggregation," *Biomed. Opt. Express*, vol. 3, no. 9, pp. 2326–2338, 2012.